Screened test-charge - electron interaction including many-body effects in two and three dimensions

1997 J. Phys.: Condens. Matter 9 3749

(http://iopscience.iop.org/0953-8984/9/18/014)

J. Phys.: Condens. Matter **9** (1997) 3749–3762. Printed in the UK PII: S0953-8984(97)79900-4

Screened test-charge–electron interaction including many-body effects in two and three dimensions

A Gold† and A Ghazali‡

† Laboratoire de Physique des Solides, Université Paul Sabatier, 118 Route de Narbonne, 31062 Toulouse, France

‡ Groupe de Physique des Solides, Universités Paris 7&6, 2 Place Jussieu, 75251 Paris, France

Received 28 November 1996

Abstract. Bound states of a *negatively* charged test particle and an electron are studied by incorporating many-body effects (exchange and correlation) in the screening function of an interacting electron gas via the local-field correction. Using a variational method and a matrix-diagonalization method we determine the energies and the wave functions of the ground state and the excited states as functions of the electron density for three-dimensional and two-dimensional systems. For high electron density no bound states are found. Below a critical density the number and the energy of the bound states increase with decreasing electron density. We also present results for bound-state energies of a *positively* charged test particle with an electron, and compare them with results obtained within the random-phase approximation where the local-field correction is ignored.

1. Introduction

It is known that the potential of a test charge screened by a three-dimensional electron gas gives rise to Friedel oscillations [1–3]. A similar effect is known in two-dimensional systems [4]. The Friedel oscillations occur already within the framework of the random-phase approximation (RPA). For two-dimensional systems it was argued recently [5] that many-body effects, described by the local-field correction (LFC), strongly modify the screening properties of the electron gas at low density. In the low-density range the screened interaction potential of two negative (or two positive) test charges was found to be strongly attractive (binding energies of order one rydberg) if many-body effects are included in the screening function via the LFC. For one-dimensional [6] and two-dimensional systems [7, 8] the binding energy of these bound states was found to be much larger than for three-dimensional systems [9]. The work described in [6–9] concerns the test-charge–test-charge interaction screened by an electron gas, and the screening is described by the dielectric function $\varepsilon_{tt}(q)$.

In this paper we study bound states for the screened test-charge–electron interaction for two- and three-dimensional systems. The essential difference from the earlier studies [6–9] is that here the screening function $\varepsilon_{te}(q)$ takes a different form to account for the indistinguishability of the electrons. We are using the Kukkonen and Overhauser approach [10] in order to treat this effect.

Our motivation for this work (as in the earlier publications [6–9]) is to understand, within a simple model and with a transparent calculation, the counterintuitive possibility of a Coulomb-interaction-induced attraction in the electron gas between two equally charged

0953-8984/97/183749+14$19.50

particles. An analytical expression for the LFC as a function of the Wigner–Seitz parameter r_s enables us to study the screened interaction as a function of electron density. Screening effects for a positively charged impurity are generally treated in the literature within the RPA and many-body effects are neglected. In some theoretical papers also the screening function for the test-charge–test-charge interaction is used. We insist here that the screening function for the test-charge–electron interaction has to be used in that case.

The paper is organized as follows. In section 2 we describe the model and the theory. Our results for negative test charges are presented in section 3 and the results for positive test charges are given in section 4. We discuss the method, the results and possible experiments in section 5. We give our conclusions in section 6.

2. The model and theory

2.1. The model: the screened Coulomb interaction

As the model we use a d-dimensional electron gas ($d = 3, 2$) with a parabolic dispersion and density N_d. Distances are expressed in units of the effective Bohr radius $a^* = \varepsilon_L/m^*e^2$ with the Planck constant $h/2\pi = 1$. Wavenumbers are expressed in units of the inverse Bohr radius. m^* is the effective mass and ε_L is the dielectric constant of the background. Energy values are expressed in units of the effective rydberg, $\mathrm{Ryd}^* = m^*e^4/2\varepsilon_L^2$. The density parameter r_s is given by $r_s = [3/4\pi N_3 a^{*3}]^{1/3}$ for three dimensions and by $r_s = [1/\pi N_2 a^{*2}]^{1/2}$ for two dimensions. $r_s a^*$ is the Wigner–Seitz radius. $N_3 = k_F^3/3\pi^2$ ($N_2 = k_F^2/2\pi$) is the electron density in three (two) dimensions and k_F is the Fermi wavenumber.

The Coulomb interaction potential in the Fourier space between two negative test charges (tt) is repulsive and is given by $V_{tt}(q) = +V(q)$ with $V(q) = 4\pi e^2/\varepsilon_L q^2$ in three dimensions and $V(q) = 2\pi e^2/\varepsilon_L q$ in two dimensions. The screened interaction potential $V_{tt,sc}(q)$ is written as

$$V_{tt,sc}(q) = \frac{V_{tt}(q)}{\varepsilon_{tt}(q)}. \tag{1a}$$

The dielectric function $\varepsilon_{tt}(q)$, calculated within the RPA and including the LFC $G(q)$, is given by [10]

$$\frac{1}{\varepsilon_{tt}(q)} = \frac{1 - V(q)G(q)X_0(q)}{1 + V(q)[1 - G(q)]X_0(q)}. \tag{1b}$$

$X_0(q)$ is the Lindhard function of the free-electron gas [1]. This screening function was used in our earlier work [7–9].

For the interaction between a negatively charged test particle (an electron) and an electron (te) the potential is given by $V_{te}(q) = +V(q)$. For a positive test charge the interaction potential is given by $V_{te}(q) = -V(q)$. The screened interaction potential $V_{te,sc}(q)$ is expressed as [10]

$$V_{te,sc}(q) = \frac{V_{te}(q)}{\varepsilon_{te}(q)} \tag{2a}$$

with

$$\varepsilon_{te}(q) = 1 + V(q)[1 - G(q)]X_0(q). \tag{2b}$$

For $G(q) = 0$ one gets the RPA expression $\varepsilon_{RPA}(q) = 1 + V(q)X_0(q)$, and $\varepsilon_{tt}(q) = \varepsilon_{te}(q) = \varepsilon_{RPA}(q)$. The difference between $\varepsilon_{te}(q)$ and $\varepsilon_{tt}(q)$ is due to the different many-body effects as described by $G(q)$: $\varepsilon_{tt}(q) > \varepsilon_{te}(q)$ and $V_{tt,sc}(q) < V_{te,sc}(q)$.

In our calculation we use for the LFC the sum-rule approximation [11] of the Singwi, Tosi, Land and Sjölander (STLS) approach [12]. For a review concerning the STLS approach, see [13]. In the STLS approach the compressibility sum rule is not fulfilled. For this reason we modified the sum-rule approach in order to fulfil the compressibility sum rule. Details will be published elsewhere [14]. The LFC is parametrized by three coefficients $C_{id}(r_s)$ $(i = 1, 2, 3)$ and has a similar form to that within the Hubbard approximation [2] where only exchange effects are taken into account. The form used for the LFC was described in reference [8] for two dimensions and in reference [9] for three dimensions. Finally, we note that this sum-rule approach is in reasonable agreement with recent Monte Carlo calculations for the screening function of the two-dimensional [15] and the three-dimensional [16] electron gas.

For the three-dimensional electron gas the LFC is written as [14]

$$G(q) = r_s^{3/4} \frac{0.846q^2}{2.188q_3^2 C_{13}(r_s) + q^2 C_{23}(r_s) - q_3 q C_{33}(r_s)} \tag{3a}$$

with $q_3 = 12^{1/4}/r_s^{3/4}a^*$. For the two-dimensional electron gas the LFC is given by [14]

$$G(q) = r_s^{2/3} \frac{1.402q}{[2.644q_2^2 C_{12}(r_s)^2 + q^2 C_{22}(r_s)^2 - q_2 q C_{32}(r_s)]^{1/2}} \tag{3b}$$

with $q_2 = 2^{1/2}/r_s^{2/3}a^*$. During the last thirty years a lot of activity has been directed towards the study of many-body effects via the LFC. A general discussion can be found in reference [13]. As long as exchange and correlation effects are included in the LFC, the specific form used for $G(q)$ in the calculation is not important for our results. This was demonstrated for the test-charge–test-charge interaction [8, 9].

2.2. Theory: the Schrödinger equation

The Schrödinger equation for the screened potential is solved numerically in the momentum space. As was shown before for the test-charge–test-charge interaction [8, 9], this method is accurate. The Schrödinger equation in the momentum space is given by

$$\frac{q^2}{2m}\psi(\boldsymbol{q}) + \frac{1}{(2\pi)^d}\int \mathrm{d}^d\boldsymbol{q}'\ V_{te,sc}(\boldsymbol{q}-\boldsymbol{q}')\psi(\boldsymbol{q}') = E\psi(\boldsymbol{q}). \tag{4}$$

We have discretized the integral over $\boldsymbol{q}'$ in equation (4) in the form of a matrix. The eigenenergy and eigenfunction problem is then solved numerically by a standard method for matrix diagonalization. Details can be found in reference [8] and reference [9]. At low electron density the matrix is ill defined for $\boldsymbol{q}' - \boldsymbol{q} = \boldsymbol{0}$, and the numerical results are less accurate in the case of an attractive test charge where the binding energy is dominated by the behaviour for $\boldsymbol{q}' \to \boldsymbol{q}$. This is important in the weakly screened case where the variational method sometimes gives a slightly larger binding energy than the numerical method.

For three dimensions the wave function $\psi(\boldsymbol{r})$ is given by $\phi_{n_r l}(r)Y_{lm}(\varphi, \theta)$ [17]. The degeneracy of these states is $g_l = 2l + 1$. $\phi_{n_r l}(r)$ is the solution of the radial Schrödinger equation for the effective potential $V_{eff}(r) = V_l(r) + V_{te,sc}(r)$ with $V_l(r) = l(l+1)/2m^*r^2$. $V_{eff}(r)$ is strongly repulsive at small distances $V_{eff}(r \to 0)/\mathrm{Ryd}^* = l(l+1)a^{*2}/r^2 + 2a^*/r$. It is clear that for $l > 0$ the behaviour of the wave function for small r is determined by $V_l(r)$, and $\phi_{n_r l}(r \to 0) \propto r^l$. In the momentum space the wave function is given by $\psi(\boldsymbol{q}) = \phi_{n_r l}(q)Y_{lm}(\theta, \varphi)$ and $\phi_{n_r l}(q \to 0) \propto q^l$.

For two dimensions we use $\psi(\boldsymbol{r}) = \phi_{n_r l}(r)\exp[\pm \mathrm{i}l\varphi]$ with degeneracy $g_l = 1$ for $l = 0$ and $g_l = 2$ for $l > 0$. $\phi_{n_r l}(r)$ is the solution of the radial Schrödinger equation for the

effective potential $V_{eff}(r) = V_l(r) + V_{te,sc}(r)$ with $V_l(r) = l^2/2m^*r^2$. In the momentum space the wave function is written as $\psi(\boldsymbol{q}) = \phi_{n_r l}(q)\exp(\pm il\varphi)$. In the following we will use $\phi(r)$ instead of $\phi_{n_r l}(r)$.

In the following we also use the trial-wave-function method, which is easy to apply if more accurate expressions for the LFC become available. In the present paper we derive estimates for the accuracy of this method by comparing with the matrix-diagonalization method. This method is numerically very demanding because no symmetry arguments have been used.

3. Negative test charges

3.1. The variational wave function

With a trial wave function $\phi_{var}(r)$ the variational energy is given by $E_{var} = \langle T\rangle + \langle V_l\rangle + \langle V_{te,sc}\rangle$. The average $\langle O\rangle = \int_0^\infty \mathrm{d}r\; r^{d-1}\phi_{var}(r)^* O\phi_{var}(r)$ for $O = T$, V_l and $V_{te,sc}$ can be calculated analytically for some trial wave functions. We use as the variational radial wave function

$$\phi_{var}(r) = Ar^{k_1/2}\mathrm{e}^{-r^2/2\alpha^2} \tag{5}$$

with the normalization constant A and the variational parameters k_1 and α. The screened repulsive potential shows a minimum as a function of r like a one-dimensional oscillator potential; this fact motivated the choice of $\phi_{var}(r)$.

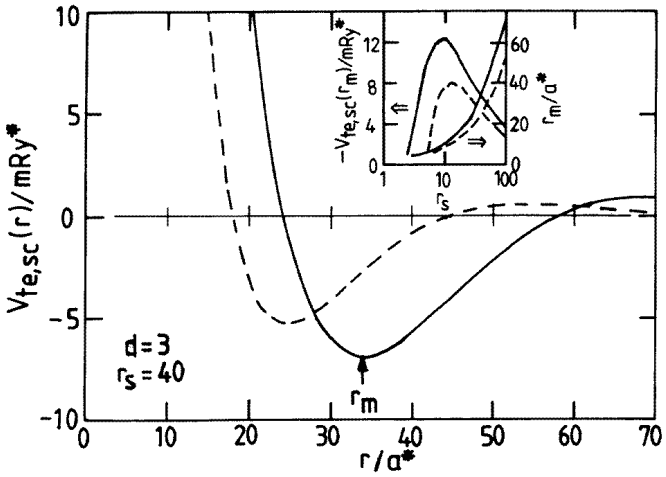

Figure 1. The screened potential $V_{te,sc}(r)$ versus distance r for $r_s = 40$ in three dimensions for a negative test charge. For the solid line the LFC is included and the dashed line represents the RPA. In the inset we show $V_{te,sc}(r_m)$ and r_m versus r_s.

The variational wave function shows a maximum at $r^* = (k_1/2)^{1/2}\alpha$. For $k_1 > 0$ the wave function has a node at $r = 0$ and we use the notation $n_r = 1$ for the radial quantum number n_r. For different values of l the notation for the state $n_r l$ is 1s, 1p or 1d. We find that the bound states are very extended in space due to the large repulsion at small distances: see the large value of r_m found for the minimum of the screened potential in figure 1. The

variational form of the radial wave function as given in equation (5) was successfully used in describing the bound states for the test-charge–test-charge interaction. For details, see references [8, 9].

3.2. Results for three dimensions

In the real space the screened Coulomb interaction in three dimensions is given by

$$V_{te,sc}(r) = \frac{1}{2\pi^2 r}\int_0^\infty \mathrm{d}q\ q\sin(qr)V_{te,sc}(q). \tag{6}$$

A representative example for $V_{te,sc}(r)$ is shown in figure 1 for $r_s = 40$ with a minimum $V_{te,sc}(r_m) = -6.93$ mRyd* at $r_m = 34.0a^*$. Note the strong Coulomb repulsion for small distances. We remark that the LFC shifts the minimum to lower energies and to larger distances as compared to the RPA. A systematic study of $V_{te,sc}(r_m)$ and r_m versus r_s is shown in the inset of figure 1. We note the strong variation of $V_{te,sc}(r_m)$ with r_s with a minimum of -12.4 mRyd* at $r_s = 9$.

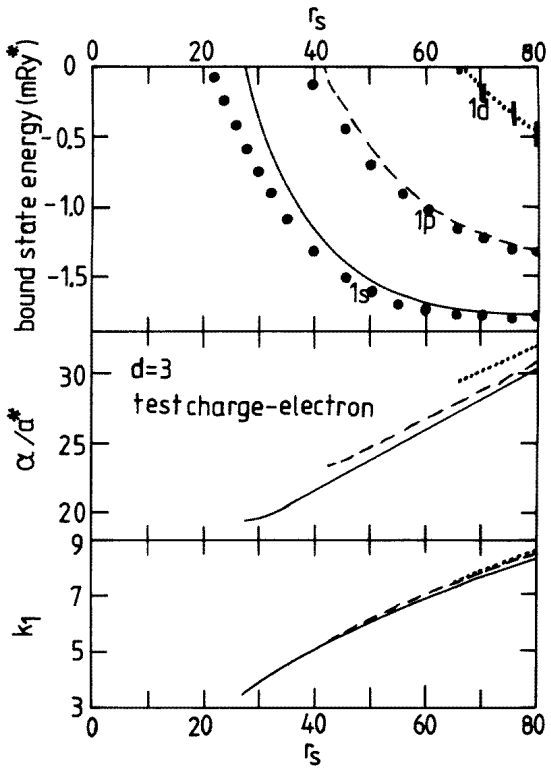

Figure 2. The minimal energy E_{min} and variational parameters α and k_1 versus r_s for $n_r = 1$ and $l = 0, 1, 2$ in three dimensions including the LFC for a negative test charge. The solid dots are the results obtained by matrix diagonalization.

Our results for the binding energy versus r_s are shown in figure 2. The binding energies are of order 1 mRyd* and the lower-lying energy states are well described by our variational method. However, when the binding energy is small, the matrix-diagonalization method

gives a larger binding energy than the variational method. For $r_s < r_{sc} = 20$ no bound state exists. Our variational results give a smaller binding energy with a critical density given by $r_{sc} = 27.5$. Figure 2 contains the complete information about the ground state and the excited states.

The variational parameters α and k_1 versus r_s are also shown in figure 2. For $r_s = 40$ we found $r^* = 34.6a^*$ for $l = 0$, which is in good agreement with r_m; see figure 1. r^* and r_m increase with increasing r_s. Note that α and k_1 are nearly independent of l which means that all of these states show a maximum at nearly the same $r^* \approx r_m$.

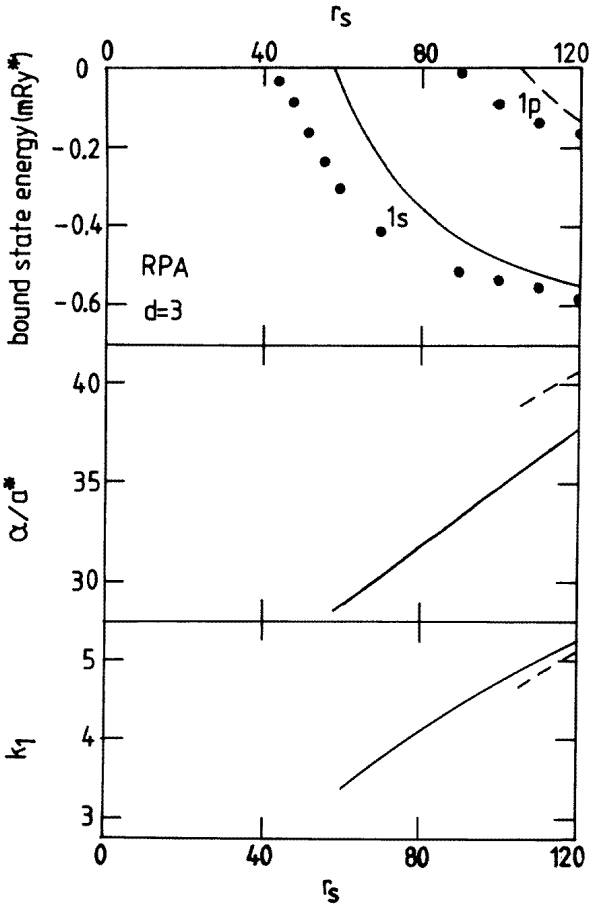

Figure 3. The minimal energy E_{min} and variational parameters α and k_1 versus r_s for $n_r = 1$ and $l = 0, 1$ in three dimensions within the RPA for a negative test charge.

Similar results are obtained within the RPA when the LFC is set to zero; see figure 3. However, the binding energy of the ground state is about a factor of 3 smaller than with the LFC and r_{sc} is much larger ($r_{sc} \approx 40$). These results are interesting from a theoretical point of view: from figure 3 we conclude that many-body effects described by the LFC are not necessary in order to obtain bound states. However, the inclusion of the LFC reduces the critical density considerably: remember that $N_3 \propto 1/r_s^3$.

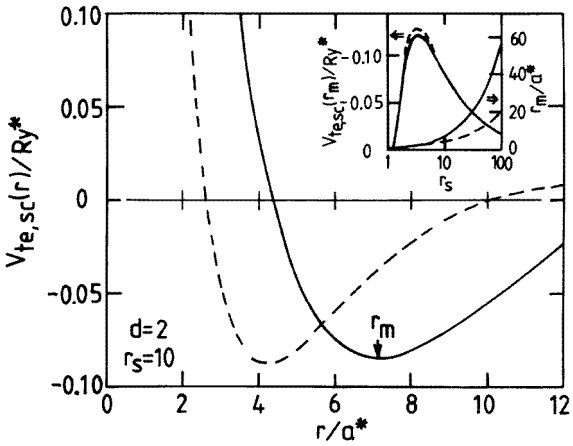

Figure 4. The screened potential $V_{te,sc}(r)$ versus the distance r for $r_s = 10$ in two dimensions for a negative test charge. For the solid line the LFC is included and the dashed line represents the RPA. In the inset we show $V_{te,sc}(r_m)$ and r_m versus r_s.

3.3. Results for two dimensions

In two dimensions the screened Coulomb interaction in the real space is given by

$$V_{te,sc}(r) = \frac{1}{2\pi}\int_0^\infty \mathrm{d}q\ q\, J_0(qr) V_{te,sc}(q). \tag{7}$$

$J_0(x)$ is the zero-order Bessel function of the first kind. A representative example for $V_{te,sc}(r)$ is shown in figure 4 for $r_s = 10$ with a minimum of $V_{te,sc}(r_m) = -85$ mRyd* at $r_m = 7.4a^*$. We remark that the LFC does not lower the minimum as compared to the RPA. A systematic study of $V_{te,sc}(r_m)$ and r_m versus r_s is shown in the inset of figure 4. We note the strong variation of $V_{te,sc}(r_m)$ with r_s with a minimum of -120.4 mRyd* at $r_s = 3.6$. It is clear that in two dimensions the attraction is a factor 10 larger than that in three dimensions; compare the insets in figure 1 and figure 4.

Our results for the binding energy versus r_s are shown in figure 5. The binding energies are of order 20 mRyd*. In general we find that the matrix-diagonalization method gives a larger binding energy than the variational method, as expected. For $r_s < r_{sc} = 4.7$ no bound state is found. Our variational results give a smaller binding energy with the critical density $r_{sc} = 5.9$.

The variational parameters α and k_1 versus r_s are also shown in figure 5. For $r_s = 10$ we find that $r^* = 7.7a^*$ for $l = 0$, which is in good agreement with r_m; see figure 4. In two dimensions the bound states are less extended in space than in three dimensions.

4. Positive test charges

4.1. The screened potential

In figure 6 we show the screened potential for a positive test charge for $r_s = 3$ and three dimensions. We present results for the test-charge–test-charge interaction, the test-charge–electron interaction, the RPA, and the Thomas–Fermi approximation (TFA). Within the TFA one uses $G(q) = 0$, and $X_0(q)$ is replaced by the density of states at the Fermi energy

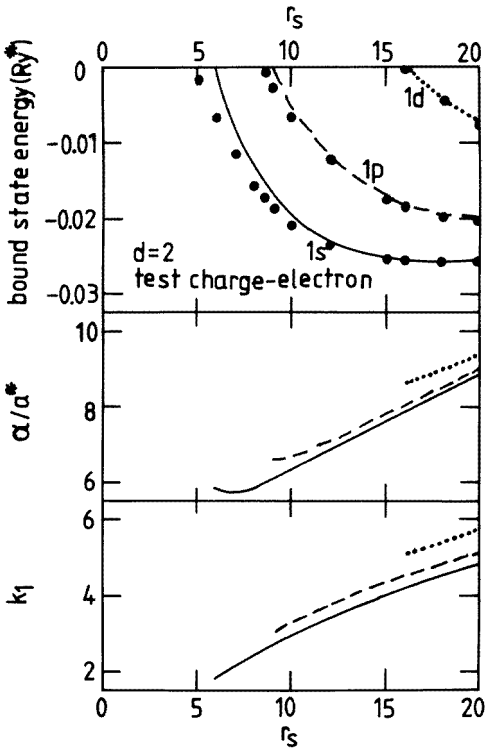

Figure 5. The minimal energy E_{min} and variational parameters α and k_1 versus r_s for $n_r = 1$ and $l = 0, 1, 2$ in two dimensions including the LFC for a negative test charge. The solid dots are the results obtained by matrix diagonalization.

$\rho_F = X_0(q = 0)$. It is important to realize that already for $r_s = 3$ important differences exist for the screened potential due to many-body effects. For normal metals the Wigner–Seitz parameter is given by $1 < r_s < 5$. We hope that figure 6 will convince experimenters to take many-body effects seriously. The small differences seen in figure 6 give rise to very different bound-state energies, as shown in the following.

4.2. The variational wave function

We apply variational wave function of the (unscreened) hydrogen atom. For the ground state, which is the 1s state, we use

$$\phi_{var}(r) = A\mathrm{e}^{-r/2\nu}. \tag{8}$$

For the first excited state, which is the 2s state, we use

$$\phi_{var}(r) = A(1 - rD)\mathrm{e}^{-r/2\kappa}. \tag{9}$$

Note that $\langle 1\mathrm{s}|2\mathrm{s}\rangle = 0$, which implies a condition for D. For the second excited state, the 2p state, we use

$$\phi_{var}(r) = Ar\mathrm{e}^{-r/2\mu}. \tag{10}$$

ν, κ and μ are the variational parameters. For details of the variational form, see reference [8] and reference [9], where the screened test-charge–test-charge interaction was studied.

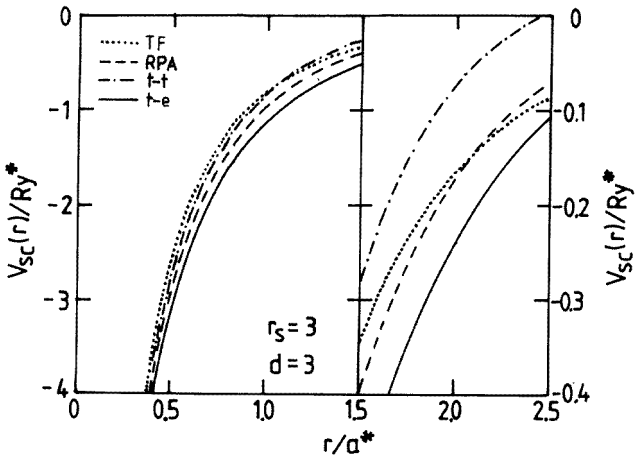

Figure 6. The screened potential $V_{sc}(r)$ versus distance r for $r_s = 3$ in three dimensions for a positive test charge. We show the results for the test-charge–test-charge interaction, the test-charge–electron interaction, the RPA, and the Thomas–Fermi approximation (TFA). On the r.h.s. an enlarged energy scale is used.

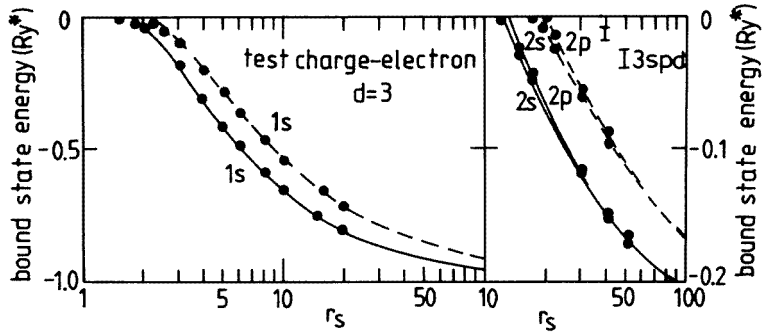

Figure 7. The minimal energy E_{min} versus r_s for the 1s state (l.h.s.) and for the 2s and 2p states (r.h.s.) in three dimensions including the LFC (solid lines) and within the RPA (dashed lines) for a positive test charge. The solid dots are the results obtained by matrix diagonalization. Some numerical results for 3s, 3p, and 3d states (with the LFC included) are shown as bars.

The equations given there can be used together with the appropriate form for the screening function $\varepsilon_{te}(q)$.

4.3. Results for three dimensions

Our results for the ground-state energy and the first excited states versus r_s are shown in figure 7. With increasing density the binding energies decrease due to screening effects and vanish at a critical density, which is Mott's density N_M [18]. Note that the 2s and the 2p states are nearly degenerate for $r_s > 30$. For very low density, $r_s = 40$ and $r_s = 50$, we also found 3s, 3p and 3d states with the matrix-diagonalization method and using the LFC; see figure 7. However, we have not studied these states in detail.

We mention that $N^{1/3}a^* = 0.62/r_s$ and, accordingly, N_M is related to a critical density parameter r_{sM}. For the ground state we obtained $r_{sM} = 2.13$ by using the RPA and $r_{sM} = 1.75$ by using the LFC. Reasonable agreement is obtained between the variational method and the matrix-diagonalization method.

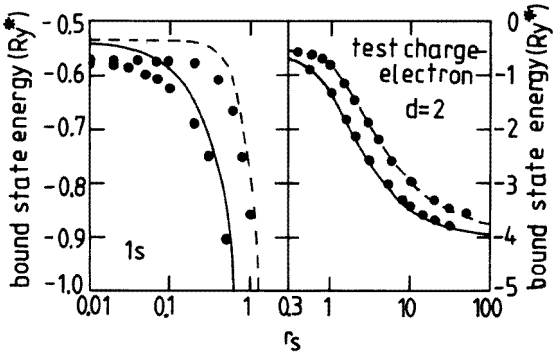

Figure 8. The minimal energy E_{min} versus r_s for the 1s state in two dimensions including the LFC (solid lines) and within the RPA (dashed lines) for a positive test charge. The solid dots are the results obtained by matrix diagonalization.

4.4. Results for two dimensions

In two dimensions the Coulomb potential screened within the RPA has a bound state for any electron density [19, 20]. A critical density (Mott's density), where the binding energy of the ground state vanishes, does not exist in two dimensions. Our results for the ground-state energy versus r_s are shown in figure 8. As found in three dimensions, the LFC increases the binding-state energy as compared to the RPA. For $r_s \to \infty$ one finds the unscreened value for the binding energy, which is -4 Ryd*.

Our results for the excited states are shown in figure 9. The LFC increases the binding energy by 50%. For $r_s \to \infty$ the unscreened value -4 Ryd$^*/9$ is obtained. The Mott density for the excited states is $r_{sM} = 11$ if the LFC is included and about $r_{sM} = 27$ within the RPA.

5. Discussion

5.1. Negative test charges

We believe that our results in three dimensions are only of theoretical interest. Normal metals are characterized by $r_s < 5$ while molecular metals such as the doped fulleride K_3C_{60} have smaller density, $r_s \approx 10$. In three-dimensional systems the bound states for the test-charge–electron interaction appear at low density. At densities $r_s > 10$ we expect that disorder effects will dominate the physical properties.

Our results obtained for two-dimensional systems might be relevant in nature for two reasons. First, by remote doping, disorder effects can be made small in heterostructures. In addition, the bound states for $r_s > r_{sc}$ have a large binding energy, and even for the test-charge–electron interaction the parameter $r_{sc} \approx 4.7$ seems accessible in two-dimensional systems. Currently used remotely doped GaAs/Al_xGa_{1-x}As heterostructures

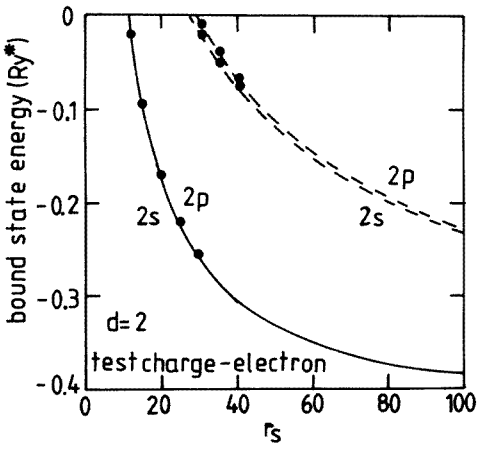

Figure 9. The minimal energy E_{min} versus r_s for the 2s and 2p states in two dimensions including the LFC (solid lines) and within the RPA (dashed lines) for a positive test charge. The solid dots are the results obtained by matrix diagonalization.

become insulating [21] due to a metal–insulator transition [22] at $r_s > 5$.

We therefore suggest the following experiment. Place a negatively charged impurity into a two-dimensional electron gas which is remotely doped in order to provide a finite electron density. For $r_s > r_{sc}$ we predict bound states between the impurity and an electron in the electron gas if disorder effects are sufficiently small. The disorder must be smaller than in the samples used in reference [21].

Table 1. For negative test charges: the critical density parameter r_{sc} and binding energy for $r_s \approx 2r_{sc}$ of the 1s state found by the variational method for two and three dimensions. The values in curly brackets are the results obtained by using the matrix-diagonalization method.

	$d = 3$		$d = 2$	
	r_{sc}	$E_{1s}(2r_{sc})$	r_{sc}	$E_{1s}(2r_{sc})$
RPA	57.0 {40}	−0.5 mRyd*	9.8 {6.8}	−10 mRyd*
Test-charge–electron	27.5 {20}	−1.3 mRyd*	5.9 {4.7}	−20 mRyd*
Test-charge–test-charge [8, 9]	8.6 {8}	−40 mRyd*	2.4 {2.1}	−350 mRyd*

The critical parameter r_{sc} for the existence of bound states can be compared with results obtained for the test-charge–test-charge interaction. The results are shown in table 1. In two-dimensional systems r_{sc} is much lower and the binding energy is much higher than in three-dimensional systems. Exchange effects present for the test-electron–electron interaction lead to a larger r_{sc} compared to that for the test-electron–test-electron interaction.

If many-body effects described by the LFC are neglected no difference exists between the test-charge–test-charge and test-charge–electron interactions, and the RPA is the relevant theory. Therefore, the RPA represents the lowest-order approximation to the above-discussed problem of the screened electron–electron interaction. In order to get the full information for the electron–electron interaction, not only the LFC for charge fluctuations but also the LFC for spin fluctuations has to be included [10]. While our calculations

for the test-charge–electron interaction give a much smaller binding energy than for the test-charge–test-charge interaction, we believe that the electron–electron interaction gives similar results to those for the test-electron–test-electron interaction; this was demonstrated in reference [5] for the two-dimensional electron gas with $r_s = 4$ and using the Hubbard approximation.

Friedel oscillations are induced by the sharpness of the Fermi surface which leads to the non-analytic behaviour of $X_0(q)$ for $q = 2k_F$. Within the RPA with $G(q) = 0$ one can replace $X_0(q)$ by $X_0(q = 0) = \rho_F$ and one obtains the TFA: Friedel oscillations and attractive parts in the screened potential are absent. If one replaces $X_0(q)$ by $X_0(q) = \rho_F/(1 + q^2/4k_F^2)$ Friedel oscillations are absent; however, attractive parts in the screened potential still exist. Therefore, we conclude that the q-dependence in the factor $[1 - G(q)]X_0(q)$ gives rise to an attractive part in $V_{te,sc}(r)$ and $V_{tt,sc}(r)$. For $V_{tt,sc}(r)$ the strength of this attractive part is determined by $G(q)$, while $G(q)$ and $X_0(q)$ determine $V_{te,sc}(r)$: by replacing $X_0(q)$ by $X_0(q) = \rho_F/(1 + q^2/4k_F^2)$ we obtain similar values for $V_{te,sc}(r_m)$ to those obtained by using the Lindhard expression for $X_0(q)$. Therefore, we believe that Friedel oscillations are not the origin of the attraction found for the screened potential.

The relevance of our calculation for possible superconductivity due to a Coulomb-interaction-induced attraction goes back to Kohn and Luttinger [23], where an electron gas with a short-range interaction has been discussed. The effective electron–electron interaction was discussed by Kukkonen and Overhauser [10] and in reference [24]. For the three-dimensional jellium model it was recently argued [25] that Coulomb-interaction-induced superconductivity should not occur for $r_s < 10$. This is in qualitative agreement with our calculation for three dimensions; see table 1. On the other hand we conclude from our results for the binding energy and for r_{sc} that in two-dimensional systems attraction should occur at higher electron density than in three dimensions. Our results for quasi-one-dimensional systems will be published elsewhere [26].

5.2. Positive test charges

Our results for a positive test charge are relevant for a charged donor screened by an electron gas and should be important for excitons, too. Our quantitative results on the effects of the LFC indicate that many-body effects must be included in the screening function. In addition, the screening function of the test-charge–electron interaction has to be used.

Table 2. For positive test charges: Mott's critical density parameter r_{sM} for the 1s, the 2s and the 2p state for the test-charge–electron interaction obtained by the variational method for two and three dimensions. The values in curly brackets are our results obtained by using the matrix-diagonalization method.

	$d = 3$		$d = 2$	
	r_{sM}(RPA)	r_{sM}(LFC)	r_{sM}(RPA)	r_{sM}(LFC)
1s state	2.1 {1.8}	1.8 {1.5}	—	—
2s state	17.8 {16.9}	12.1 {11.5}	26.6 {26}	11.2 {11}
2p state	19.8 {19.5}	12.9 {12.4}	28.8 {29}	11.2 {11}

The results concerning Mott's parameter r_{sM} for the vanishing of the bound state are summarized in table 2 for the ground state (1s) and the excited states (2s, 2p). Large shifts due to many-body effects are found for r_{sM} for the excited states. For three dimensions most

previous calculations [27, 28] of r_{sM} have been performed within the variational approach and for the ground state only.

6. Conclusion

We studied the screened test-charge–electron interaction assuming a test particle with negative charge. The bound-state energies found in the low-electron-density range for $r_s > r_{sc}$ are smaller than for the test-charge–test-charge interaction. Our calculation shows that with decreasing system dimension the binding energy increases, and in the two-dimensional electron gas, bound states can be expected at a moderate density ($r_s > 5$). In this paper we compared results for r_{sc} obtained for the test-charge–electron interaction and the test charge–test-charge interaction including many-body effects via the LFC.

For a test particle with a positive charge, many-body effects are important—however, only at a quantitative level. If many-body effects are taken into account, the binding energy increases by more than 20% for $0.5 < r_s < 10$. For excited states we find that Mott's parameter r_{sM} is strongly reduced by many-body effects.

Acknowledgment

The 'Laboratoire de Physique des Solides' and the 'Groupe de Physique des Solides' are 'Laboratoires associés au Centre National de la Recherche Scientifique (CNRS)'.

References

[1] Pines D and Nozières P 1966 *The Theory of Quantum Liquids* vol 1 (New York: Benjamin)
[2] Mahan G D 1990 *Many-Particle Physics* (New York: Plenum)
[3] Friedel J 1953 *Adv. Phys.* **3** 446
[4] Stern F 1973 *Phys. Rev. Lett.* **30** 278
[5] Gold A 1994 *Phil. Mag. Lett.* **70** 141
[6] Calmels L and Gold A 1995 *Phys. Rev.* B **51** 11 622
[7] Ghazali A and Gold A 1995 *Phys. Rev.* B **52** 16 634
[8] Gold A and Ghazali A 1996 unpublished
[9] Gold A and Ghazali A 1996 *J. Phys.: Condens. Matter* **8** 7393
[10] Kukkonen C A and Overhauser A W 1979 *Phys. Rev.* B **20** 550
[11] Gold A and Calmels L 1993 *Phys. Rev.* B **48** 11 622
[12] Singwi K S, Tosi M P, Land R H and Sjölander A 1968 *Phys. Rev.* **176** 589
[13] Singwi K S and Tosi M P 1981 *Solid State Physics* vol 36 (New York: Academic) p 177
[14] Gold A 1997 *Z. Phys.* B **105** at press
[15] Moroni S, Ceperley D M and Senatore G 1990 *Phys. Rev. Lett.* **64** 303
[16] Bowen C, Sugiyama G and Alder B J 1994 *Phys. Rev.* B **50** 14 838
[17] Landau L and Lifshitz E 1966 *Mécanique Quantique* (Moscow: Editions Mir)
[18] Mott N F 1949 *Proc. Phys. Soc.* **162** 416
[19] Bastard G 1980 *Phys. Rev.* B **24** 4714
[20] Hipólito O and Campos V P 1979 *Phys. Rev.* B **19** 3083
Brum J A, Bastard G and Guillemot C 1984 *Phys. Rev.* B **30** 905
Ackleh E S, Mahan G D and Wu J-W 1994 *Mod. Phys. Lett.* **8** 1041
[21] Jiang C, Tsui D C and Weimann G 1988 *Appl. Phys. Lett.* **53** 1533
Ernst S, Goni A R, Syassen K and Eberl K 1994 *Phys. Rev. Lett.* **72** 4029
[22] Gold A 1989 *Appl. Phys. Lett.* **54** 2100
Efros A L 1989 *Solid State Commun.* **70** 253
Gold A 1991 *Phys. Rev.* B **44** 8818
[23] Kohn W and Luttinger J M 1965 *Phys. Rev. Lett.* **15** 525
[24] Vignale G and Singwi K S 1985 *Phys. Rev.* B **32** 2156

[25] Richardson C F and Ashcroft N W 1996 *Phys. Rev.* B **54** R764
[26] Calmels L and Gold A 1997 *Phys. Rev.* B **55** submitted
[27] Krieger J B and Nightingale M 1971 *Phys. Rev.* B **4** 1266
[28] Greene R L, Aldrich C and Bajaj K K 1977 *Phys. Rev.* B **15** 2217
Aldrich C 1977 *Phys. Rev.* B **16** 2723
Borges A N O, Hipólito O and Campos V B 1995 *Phys. Rev.* B **52** 1724